Applied Physics Letters ARTICLE pubs.aip.org/aip/apl

Catalyst-free in-plane growth of high-quality ultra-thin InSb nanowires

Cite as: Appl. Phys. Lett. **125**, 223104 (2024); doi: 10.1063/5.0223513
Submitted: 14 June 2024 · Accepted: 15 November 2024 ·
Published Online: 26 November 2024

Fengyue He,[1,2] Lianjun Wen,[1] Xiyu Hou,[1,2] Lin-Han Li,[1,2] Lei Liu,[1] Ran Zhuo,[1] Ping-Heng Tan,[1,2] Dong Pan,[1,2,a)] and Jianhua Zhao[1,2,a)]

AFFILIATIONS

[1]State Key Laboratory of Superlattices and Microstructures, Institute of Semiconductors, Chinese Academy of Sciences, Beijing 100083, China

[2]Center of Materials Science and Optoelectronics Engineering, University of Chinese Academy of Sciences, Beijing 100049, China

[a)]**Authors to whom correspondence should be addressed:** pandong@semi.ac.cn and jhzhao@semi.ac.cn

ABSTRACT

InSb nanowires (NWs) show an important application in topological quantum computing owing to their high electron mobility, strong spin–orbit interaction, and large *g* factor. Particularly, ultra-thin InSb NWs are expected to be used to solve the problem of multiple sub-band occupation for the detection of Majorana fermions. However, it is still difficult to epitaxially grow ultra-thin InSb NWs due to the surfactant effect of Sb. Here, we develop an in-plane self-assembled technique to grow catalyst-free ultra-thin InSb NWs on Ge(001) substrates by molecular-beam epitaxy. It is found that ultra-thin InSb NWs with a diameter as small as 17 nm can be obtained by this growth manner. More importantly, these NWs have aspect ratios of 40–100. We also find that the in-plane InSb NWs always grow along the [110] and [1$\bar{1}$0] directions, and they have the same {111} facets, which are caused by the lowest-surface energy of {111} crystal planes for NWs grown with a high Sb/In ratio. Detailed structural studies confirm that InSb NWs are high-quality zinc blende crystals, and there is a strict epitaxial relationship between the InSb NW and the Ge substrate. The in-plane InSb NWs have a similar Raman spectral linewidth compared with that of the single-crystal InSb substrate, further confirming their high crystal quality. Our work provides useful insights into the controlled growth of in-plane catalyst-free III–V NWs.

Narrow bandgap semiconductors have been extensively investigated for their broad applications in infrared optoelectronics and quantum computing.[1–4] In particular, nanowires (NWs) of InSb are ideal materials for studying Majorana zero modes (MZMs) owing to their high electron mobility, strong spin–orbit interaction, and giant *g* factor.[5,6] To enable such application, it is extremely needed to grow high-quality ultra-thin InSb NWs because fewer even a single sub-band occupation is expected to be achieved in ultra-thin NW devices, which facilitates the study of MZMs.[7–9] Up to now, much work has been done to grow high-quality InSb NWs by free-standing[10–26] and in-plane growth manners.[27,28] However, the reported InSb NWs grown by these two growth manners often show a large diameter (~100 nm), and it is still difficult to obtain ultra-thin InSb NWs. On the one hand, it is difficult to grow free-standing ultra-thin InSb NWs with high aspect ratios since the surfactant effect of Sb can enhance the lateral growth and suppress the axial growth of the InSb NWs.[24,29] On the other hand, for InSb NWs grown by the in-plane selective-area epitaxy, the diameter of the InSb NW is defined by the size of channel pattern. As a result, due to the limitation of nanofabrication, the diameter of NWs is typically larger than 100 nm.[4,27,28,30–36] These unexpected results are hindering the study of topological physics based on InSb NWs. It has become increasingly urgent to develop a technique for preparing high-quality ultra-thin InSb NWs.

In this work, we demonstrate the growth of ultra-thin InSb NWs using the in-plane self-assembled technique by molecular-beam epitaxy (MBE). It is found that in-plane ultra-thin InSb NWs with a diameter as small as 17 nm can be grown. Moreover, these InSb NWs have high aspect ratios, and they preferentially grow along the [110] and [1$\bar{1}$0] directions with the same {111} facets surface morphology. All in-plane InSb NWs are high-quality zinc blende crystals, and there is a strict epitaxial relationship between the NW and the substrate. The high crystal quality of InSb NWs was further confirmed by the Raman spectroscopy measurements. Our work lays the foundation for the development of high-performance InSb NW electronic and quantum devices.

InSb NWs were grown in a solid source MBE system (VG V80H). Commercial Ge(001) wafers were used as the substrates. The

substrate temperature is measured by the thermocouple. The Sb cell is a standard Knudsen cell, and the Sb species is Sb_4. Before the NW growth, the natural oxide layer of Ge(001) substrates was removed by thermal annealing at 510 °C for 5 min. Stripe-shaped grooves can appear on the Ge (001) substrates during the substrates were heated and annealed.[37,38] The size of the grooves in this work is much smaller than that of the Ge substrate annealed at high temperatures in the literatures.[37,39–41] All the in-plane InSb NWs were grown on these grooves. The formation of the groove is related to the minimization of surface energy. Detailed formation process of the grooves will be discussed later. We have systematically investigated the influences of growth parameters on the morphology of InSb NWs (see Figs. S1–S4). We find that the optimum growth parameters are as follows: the growth temperature is 460 °C. The In and Sb beam equivalent pressures (BEPs) are 4.5×10^{-9} and 3.6×10^{-7} mbar, respectively. The corresponding Sb/In flux BEP ratio is 80. All our samples were grown for 45 min. The morphologies of the InSb NWs were examined by a scanning electron microscope (SEM) in the FEI Nova NanoSEM 650 system. To analyze the microstructure of InSb NWs, cross-sectional lamellae were prepared using a standard lift-out method in the FEI Helios G4 CX FIB system. The crystal structure was examined by high-resolution transmission electron microscopy (HRTEM) and high-angle annular dark-field scanning transmission electron microscopy (HAADF-STEM) in the JEM F200 system. The compositional distribution of NWs was also measured by the energy dispersive spectrum (EDS) attached to the JEM-F200. In addition, the Raman spectra of NWs were measured at room temperature using the Jobin-Yvon HR-Evolution micro-Raman system. The spot size of the laser beam used for the Raman measurements is 1 μm.

As mentioned earlier, it is still difficult to obtain ultra-thin InSb NWs, which is hindering the study of MZMs based on InSb NWs. To solve this problem, here, we develop an in-plane self-assembled technique to grow ultra-thin InSb NWs. Figures 1(a) and 1(b) show the SEM images of the in-plane InSb NWs. It is found that ultra-thin InSb NWs can be obtained by this growth manner. As shown in Fig. 1(a), the in-plane InSb NW has an ultra-thin diameter of 17 nm and a high aspect ratio of 100. According to literatures,[5,10,14,15,21,22,24,27,28] InSb NWs with a high aspect ratio can be grown with vapor–liquid–solid and SAG methods, but their diameter is relatively large (see Table S1). In our work, in-plane assembled InSb NWs not only have an ultra-thin diameter but also have a high aspect ratio. We note that in-plane InSb NWs always grow along the ⟨110⟩ directions on the Ge (001) substrates (see Fig. S5). Moreover, [110]- and [1$\bar{1}$0]-oriented InSb NWs exhibit the same surface morphology when they have the same diameter [see Fig. 1(b)]. These results are different from that of in-plane III–V NWs grown by selective-area epitaxy,[27,28,30,31] where rectangular or pyramidal cross sections were observed. We believe that these differences should be related to the different growth mechanisms of the NWs, and it will be discussed later. Figure 1(c) shows the statistical data of the diameter and the aspect ratio of the in-plane InSb NWs. It can be seen that the yield of NWs with a diameter less than 50 nm is over 60%. At the same time, these ultra-thin NWs also exhibit a high aspect ratio (40–100). The preparation of the ultra-thin InSb NWs with a high aspect ratio is beneficial for the fabrication of the InSb NW devices.

The crystal quality and compositional distribution are key parameters that determine the performance of NW devices. Hence, the microstructure of InSb NWs is further studied by TEM and EDS. It is found that all InSb NWs are pure zinc blende single crystals. Figures 2(a)–2(f) show the microstructure of a [110]-oriented InSb NW with a diameter of 93 nm. We can see from Fig. 2(a) that this NW shows a pyramidal cross section, and its sidewalls mainly consist of {111} facets. We also note that the sidewalls of [1$\bar{1}$0]-oriented NWs are composed of {111} facets (see Fig. S6), which further suggests that the growth mechanism of our NWs is different from that of NWs grown by in-plane selective-area epitaxy. Figures 2(b) and 2(c) show that the NW has a pure zinc blende phase, and there is a strict epitaxial relationship between the NW and the substrate. At the heterointerface, the strain is relaxed by periodic dislocations [see Fig. 2(d)]. EDS maps further prove that there is a clear interface between the NW and the substrate [see Figs. 2(e) and 2(f)]. It is worth noting that few planar defects such as twins and stacking faults are also observed in some samples. The occurrence of such defects may be related to the surface flatness of the substrate and the lattice mismatch between the NW and the substrate

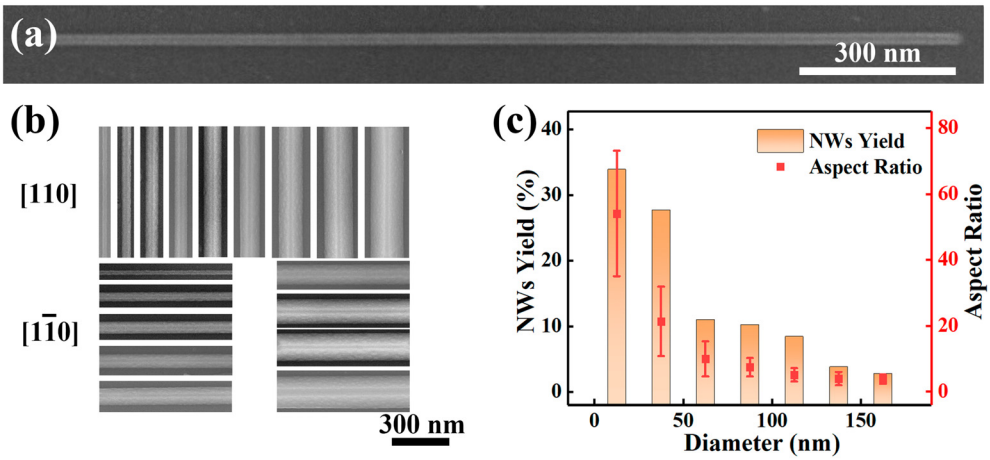

FIG. 1. (a) SEM image of an ultra-thin in-plane InSb NW grown on the Ge (001) substrate. (b) Magnified SEM images of the [110] and [1$\bar{1}$0]-oriented in-plane InSb NWs grown on the Ge (001) substrate. (c) The statistical data of the diameter and the aspect ratio of the in-plane InSb NWs. 389 NWs were counted.

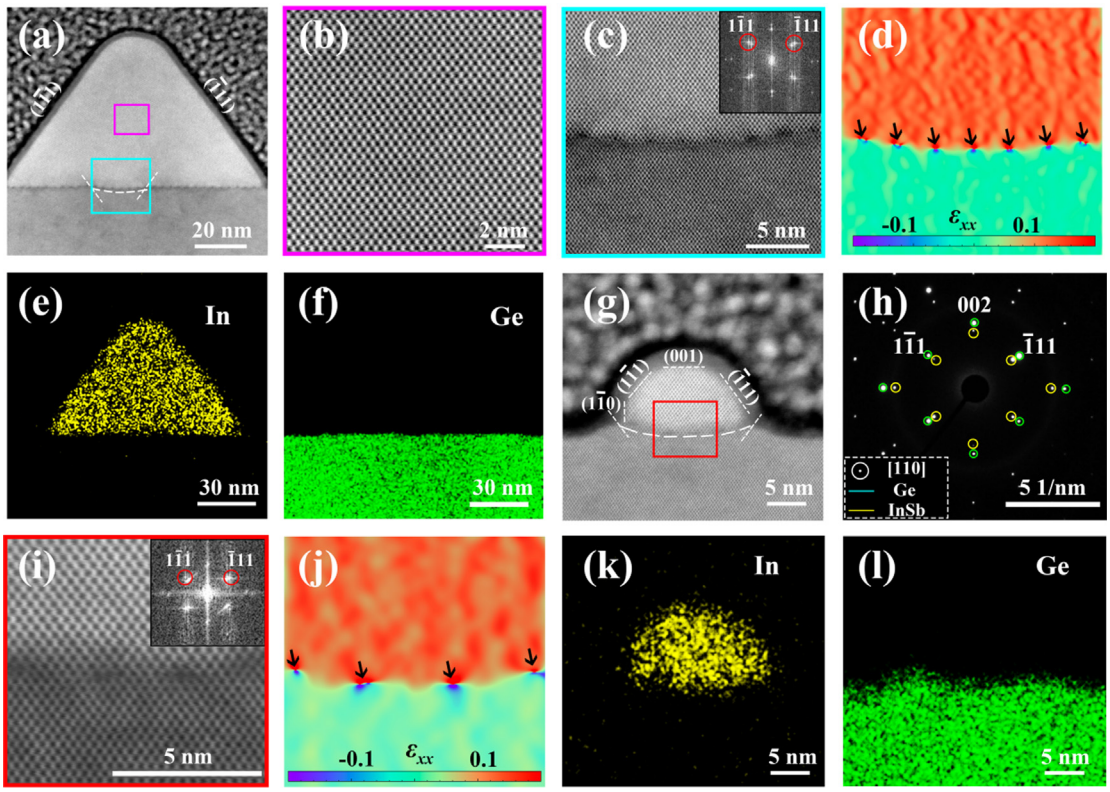

FIG. 2. (a) Cross-sectional HAADF-STEM image of a [110]-oriented InSb NW with a diameter of 93 nm. (b) and (c) HAADF-STEM images taken from the middle section of InSb and InSb/Ge interface region in panel (a), respectively. The inset in panel (c) is its fast Fourier transform (FFT) image. (d) The strain map of panel (c) obtained through geometrical phase analysis (GPA). (e) and (f) False color EDS maps of the InSb NW. (g) Cross-sectional HAADF-STEM image of a [110]-oriented NW with a diameter of 17 nm. (h) The selected area electron diffraction (SAED) patterns of the InSb NW and Ge substrate. (i) HAADF-STEM image taken from InSb/Ge interface region in panel (g). The inset in panel (i) is its FFT image. (j) The strain map of panel (i). (k) and (l) False color EDS maps of the InSb NWs. The rectangles in panels (a) and (g) highlight the regions where the high-resolution TEM images were recorded.

(see Fig. S6). The aforesaid results prove that high-quality InSb NWs can be obtained by the in-plane self-assembled technique.

As mentioned earlier, reducing the diameter of InSb NWs to the value of much less than its exciton Bohr radius (61 nm)[42,43] is the key to achieving a fewer even single sub-band occupation. Therefore, we further study the microstructure of the ultra-thin InSb NWs. Figure 2(g) shows the cross-sectional HAADF-STEM image of a [110]-oriented InSb NW with a diameter of 17 nm. Obviously, this ultra-thin InSb NW is still a pure zinc blende single crystal, and there is a clear interface and strict epitaxial relationship between the NW and the substrate [see Figs. 2(g)–2(l)]. Differently, the ultra-thin InSb NW shows a mesa-like cross section shape. Interestingly, we also note that although the diameters of thick and thin NWs shown in Figs. 2(a) and 2(g) are quite different, these NWs are always grown from a groove with the similar size [the groove is indicated by white dashed lines in Figs. 2(a) and 2(g)]. We conjecture that these phenomena should be related to the growth mechanism of the in-plane InSb NWs. The details will be discussed later.

Miro-Raman spectroscopy can provide specific information about lattice vibrations (phonon modes), which can be used to further

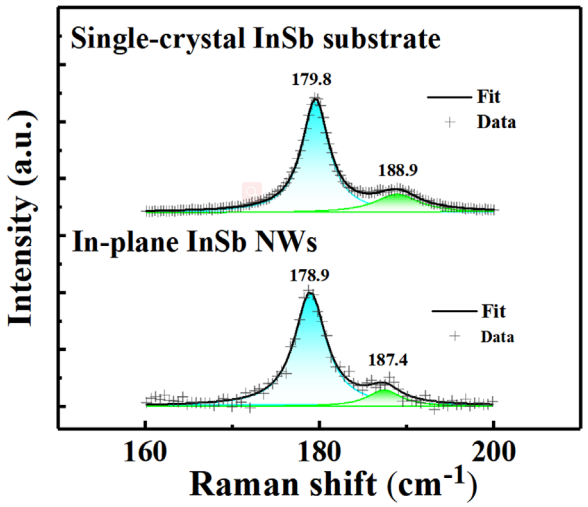

FIG. 3. Raman spectra of the in-plane InSb NWs and single-crystal InSb substrate.

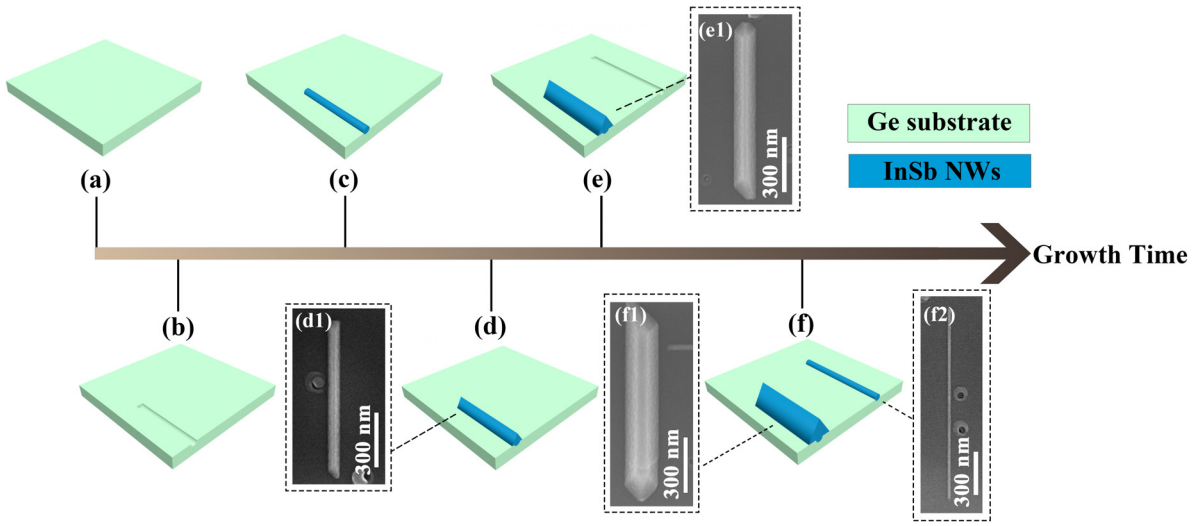

FIG. 4. Schematic diagrams of the in-plane InSb NW growth process. (a) Ge (001) substrate. (b) A groove is formed during the annealing process of the substrate. (c) and (d) The InSb NW grown in the groove continuously. (e) A new groove is formed. (f) The InSb NW grown both in the old and new grooves continuously. (d1)–(e1) SEM images of the typical in-plane InSb NWs in the different growth stages.

evaluate the phase purity of InSb NWs. Figure 3 shows the Raman spectra of the in-plane InSb NWs and InSb single-crystal substrate at room temperature in which the InSb single-crystal substrate is used as the reference sample. The Raman spectrum of InSb NWs has two peaks at 178.9 and 187.4 cm^{-1} extracted from a Lorentzian fit. The two peaks correspond to the transverse optical (TO) and longitudinal optical (LO) phonon modes of InSb, and the corresponding modes of the InSb single-crystal substrate are located at 179.8 and 188.9 cm^{-1}, respectively. The slight difference between the peak positions of the InSb NWs and the InSb single-crystal substrate has also been observed in the previous reports, which is explained by the strain[44] or the quantum confinement effect.[23,45–47] In our case, the strain is completely relaxed by forming the periodic dislocation at the InSb/Ge interface [see Figs. 2(d) and 2(j)]. Therefore, we conjecture that the redshift of the Raman peak of InSb NWs is related to the quantum confinement effect in NWs. The full width at half maximum (FWHM) of TO phonon modes for InSb NWs (4.6 cm^{-1}) is also similar to that (3.7 cm^{-1}) of InSb single-crystal substrate further demonstrating high crystal quality for our NWs. The slightly increased FWHM mainly results from spectral broadening due to the quantum confinement effect[23,45–47] and a few dislocations and planar defects in InSb NWs as that observed in TEM images (Fig. S6).[46,48]

Finally, we discuss the growth process/mechanism of the in-plane InSb NWs. As mentioned earlier, the growth mechanism of in-plane InSb NWs in this work is quite different from that of the InSb NWs grown with the routine manners. Traditionally, free-standing InSb NWs grown with a vapor–liquid–solid mechanism and a metal catalyst are essential during the NW growth. For InSb NWs grown with in-plane selective-area-epitaxy, an amorphous mask is indispensable for NW growth. In our work, no metal catalysts are used before NW growth, and spherical alloy particles are also not observed on the top of in-plane InSb NWs. It indicates that the growth mechanism of our in-plane InSb NWs is not the traditional vapor–liquid–solid mechanism. In addition, no amorphous mask was fabricated on the Ge substrates before NW sample growth, which means that our in-plane InSb NWs were not grown with the selective-area-epitaxy manner. It is worth mentioned that the Ge substrates were annealed at high temperatures before InSb NW growth, and grooves can be clearly observed at the InSb/Ge interface regions. Thus, we conjecture that in-plane InSb NWs in this work are grown with a groove-guided manner. Figure 4 shows the schematic diagrams of the in-plane InSb NW growth process. As shown in Figs. 4(a) and 4(b), the groove is first formed during the thermal annealing process of Ge (001) substrates. It may provide the nucleation site for NW growth.[49–51] The formation of the groove should be related to the minimization of surface energy,[37,39] and detailed discussions are shown in Figs. S7 and S8. As a result, grooves are easily formed along the <110> directions. After that, the growth of in-plane NWs is initiated by opening the In and Sb shutters [see Fig. 4(c)]. Because of the curved morphology of the groove on the Ge (001) substrate, the competitive growth of different crystal faces such as {111}, {110}, and {100} occurs at this stage [see Fig. 2(g)], which makes the NWs show a mesa-like surface morphology [see Fig. S9(a)]. As the NW growth continues, the diameter of NWs gradually increases [see Fig. 4(d)]. Without the constraint of the groove, the lowest-surface-energy {111} planes quickly become the dominant crystal planes [see Fig. S9(b)] under growth conditions of a high Sb/In ratio,[52] ultimately resulting in the formation of a pyramidal surface morphology of NWs [see Fig. 2(a)]. At the same time, new grooves will be formed in this stage [see Fig. 4(e)]. Then, new NWs can be obtained in these new grooves [see Fig. 4(f)]. When the NW growth is terminated, the in-plane NWs with different surface morphology are obtained simultaneously (see Figs. 1 and 2).

In summary, we demonstrate the in-plane growth of ultra-thin InSb NWs on Ge (001) substrates using the catalyst-free self-assembled technique by MBE. It is found that ultra-thin InSb NWs with high aspect ratios can be obtained. In-plane InSb NWs always grow along the [110] and [1$\bar{1}$0] directions, and they have the same {111} facets, which are caused by the lowest-surface energy of {111} crystal planes

for NWs grown with a high Sb/In ratio. Detailed structural studies prove that all InSb NWs are high-quality single crystals, and there is a strict epitaxial relationship between the InSb NW and the Ge substrate. At the heterointerface, the strain is released by forming the periodic dislocations. In addition, the Raman spectroscopy has a narrow spectral linewidth, which further confirms that the in-plane InSb NWs have high crystal quality. The fabrication of ultra-thin high-quality in-plane InSb NWs provides opportunities for the development of InSb-based devices for applications in nanoelectronics, optoelectronics, and quantum electronics and for the study of fundamental physical phenomena.

See the supplementary material for details on investigation of the influence of the growth parameters on the morphology of the in-plane InSb NWs; SEM images and volume information of the in-plane InSb NWs; summary of the catalyst, stem, diameter, aspect ratio, and growth method information for the InSb NWs in literatures and this work; cross-sectional HAADF-STEM image of a $[1\bar{1}0]$-oriented InSb NW; discussion on the possible formation process of the grooves on Ge (001) substrates; possible evolution processes of the in-plane InSb NWs with different diameters.

This work was supported by the National Natural Science Foundation of China (Grant Nos. 12374459, 61974138, and 92065106), the Innovation Program for Quantum Science and Technology (Grant No. 2021ZD0302400), and the Strategic Priority Research Program of Chinese Academy of Sciences (Grant No. XDB0460000). D.P. acknowledges the support from Youth Innovation Promotion Association, Chinese Academy of Sciences (Nos. 2017156 and Y2021043).

AUTHOR DECLARATIONS

Conflict of Interest

The authors have no conflicts to disclose.

Author Contributions

Fengyue He: Conceptualization (equal); Data curation (lead); Formal analysis (lead); Investigation (lead); Software (equal); Writing – original draft (lead); Writing – review & editing (supporting). **Lianjun Wen:** Data curation (supporting); Formal analysis (supporting); Investigation (supporting); Methodology (supporting); Software (supporting); Writing – original draft (equal); Writing – review & editing (supporting). **Xiyu Hou:** Data curation (supporting); Formal analysis (supporting); Investigation (supporting); Software (supporting); Writing – original draft (supporting). **Lin-Han Li:** Data curation (equal); Formal analysis (supporting); Investigation (supporting); Software (supporting); Writing – original draft (supporting). **Lei Liu:** Investigation (supporting); Writing – original draft (supporting). **Ran Zhuo:** Investigation (supporting); Writing – original draft (supporting). **Ping-Heng Tan:** Data curation (supporting); Formal analysis (supporting); Funding acquisition (equal); Investigation (supporting); Writing – original draft (equal); Writing – review & editing (equal). **Dong Pan:** Conceptualization (lead); Formal analysis (equal); Funding acquisition (lead); Investigation (supporting); Project administration (lead); Supervision (equal); Writing – original draft (equal); Writing – review & editing (lead). **Jianhua Zhao:** Conceptualization (equal); Formal analysis (equal); Funding acquisition (equal); Project administration (equal); Supervision (lead); Writing – original draft (equal); Writing – review & editing (equal).

DATA AVAILABILITY

The data that support the findings of this study are available from the corresponding authors upon reasonable request.

REFERENCES

[1]Z. I. Alferov, Semiconductors **32**(1), 1–14 (1998).
[2]R. M. Lutchyn, J. D. Sau, and S. Das Sarma, Phys. Rev. Lett. **105**, 077001 (2010).
[3]Y. Oreg, G. Refael, and F. von Oppen, Phys. Rev. Lett. **105**, 177002 (2010).
[4]X. Yuan, D. Pan, Y. Zhou, X. Zhang, K. Peng, B. Zhao, M. Deng, J. He, H. H. Tan, and C. Jagadish, Appl. Phys. Rev. **8**, 021302 (2021).
[5]M. T. Deng, C. L. Yu, G. Y. Huang, M. Larsson, P. Caroff, and H. Q. Xu, Nano Lett. **12**, 6414 (2012).
[6]V. Mourik, K. Zuo, S. M. Frolov, S. R. Plissard, E. P. A. M. Bakkers, and L. P. Kouwenhoven, Science **336**, 1003 (2012).
[7]C. Moore, T. D. Stanescu, and S. Tewari, Phys. Rev. B **97**, 165302 (2018).
[8]A. Vuik, B. Nijholt, A. R. Akhmerov, and M. Wimmer, Scipost Phys. **7**, 61 (2019).
[9]D. Pan, H. Song, S. Zhang, L. Liu, L. Wen, D. Liao, R. Zhuo, Z. Wang, Z. Zhang, S. Yang, J. Ying, W. Miao, R. Shang, H. Zhang, and J. Zhao, Chin. Phys. Lett. **39**, 058101 (2022).
[10]P. Caroff, J. B. Wagner, K. A. Dick, H. A. Nilsson, M. Jeppsson, K. Deppert, L. Samuelson, L. R. Wallenberg, and L.-E. Wernersson, Small **4**, 878 (2008).
[11]P. Caroff, M. E. Messing, B. M. Borg, K. A. Dick, K. Deppert, and L.-E. Wernersson, Nanotechnology **20**, 495606 (2009).
[12]D. Ercolani, F. Rossi, A. Li, S. Roddaro, V. Grillo, G. Salviati, F. Beltram, and L. Sorba, Nanotechnology **20**, 505605 (2009).
[13]L. Lugani, D. Ercolani, F. Rossi, G. Salviati, F. Beltram, and L. Sorba, Cryst. Growth Des. **10**, 4038 (2010).
[14]L. Lugani, D. Ercolani, F. Beltram, and L. Sorba, J. Cryst. Growth **323**, 304 (2011).
[15]A. T. Vogel, J. de Boor, M. Becker, J. V. Wittemann, S. L. Mensah, P. Werner, and V. Schmidt, Nanotechnology **22**, 015605 (2011).
[16]S. R. Plissard, D. R. Slapak, M. A. Verheijen, M. Hocevar, G. W. G. Immink, I. van Weperen, S. Nadj-Perge, S. M. Frolov, L. P. Kouwenhoven, and E. P. A. M. Bakkers, Nano Lett. **12**, 1794 (2012).
[17]C. Thelander, P. Caroff, S. Plissard, and K. A. Dick, Appl. Phys. Lett. **100**, 232105 (2012).
[18]B. M. Borg and L.-E. Wernersson, Nanotechnology **24**, 202001 (2013).
[19]A. Li, N. V. Sibirev, D. Ercolani, V. G. Dubrovskii, and L. Sorba, Cryst. Growth Des. **13**, 878 (2013).
[20]S. R. Plissard, I. van Weperen, D. Car, M. A. Verheijen, G. W. G. Immink, J. Kammhuber, L. J. Cornelissen, D. B. Szombati, A. Geresdi, S. M. Frolov, L. P. Kouwenhoven, and E. P. A. M. Bakkers, Nat. Nanotechnol. **8**, 859 (2013).
[21]D. Pan, D. X. Fan, N. Kang, J. H. Zhi, X. Z. Yu, H. Q. Xu, and J. H. Zhao, Nano Lett. **16**, 834 (2016).
[22]H. So, D. Pan, L. Li, and J. Zhao, Nanotechnology **28**, 135704 (2017).
[23]M. Xue, D. Pan, J. Zhao, and J. Chen, Adv. Mater. **35**, 2208952 (2023).
[24]G. Badawy, S. Gazibegovic, F. Borsoi, S. Heedt, C.-A. Wang, S. Koelling, M. A. Verheijen, L. P. Kouwenhoven, and E. P. A. M. Bakkers, Nano Lett. **19**, 3575 (2019).
[25]H. D. Park, S. M. Prokes, M. E. Twigg, Y. Ding, and Z. L. Wang, J. Cryst. Growth **304**, 399 (2007).
[26]A. T. Vogel, J. de Boor, J. V. Wittemann, S. L. Mensah, P. Werner, and V. Schmidt, Cryst. Growth Des. **11**, 1896 (2011).
[27]P. Aseev, G. Wang, L. Binci, A. Singh, S. Marti-Sanchez, M. Botifoll, L. J. Stek, A. Bordin, J. D. Watson, F. Boekhout, D. Abel, J. Gamble, K. Van Hoogdalem, J. Arbiol, L. P. Kouwenhoven, G. de Lange, and P. Caroff, Nano Lett. **19**, 9102 (2019).

[28]L. Desplanque, A. Bucamp, D. Troadec, G. Patriarche, and X. Wallart, J. Cryst. Growth **512**, 6 (2019).
[29]E. A. Anyebe, M. K. Rajpalke, T. D. Veal, C. J. Jin, Z. M. Wang, and Q. D. Zhuang, Nano Res. **8**, 1309 (2015).
[30]F. Krizek, J. E. Sestoft, P. Aseev, S. M.-S. Anchez, S. Vaitiekenas, L. Casparis, S. A. Khan, Y. Liu, T. Stankevic, A. M. Whiticar, A. Fursina, F. Boekhout, R. Koops, E. Uccelli, L. P. Kouwenhoven, C. M. Marcus, J. Arbiol, and P. Krogstrup, Phys. Rev. Mater. **2**, 093401 (2018).
[31]P. Aseev, A. Fursina, F. Boekhout, F. Krizek, J. E. Sestoft, F. Borsoi, S. Heedt, G. Wang, L. Binci, S. Marti-Sanchez, T. Swoboda, R. Koops, E. Uccelli, J. Arbiol, P. Krogstrup, L. P. Kouwenhoven, and P. Caroff, Nano Lett. **19**, 218 (2019).
[32]J. S. Lee, S. Choi, M. Pendharkar, D. J. Pennachio, B. Markman, M. Seas, S. Koelling, M. A. Verheijen, L. Casparis, K. D. Petersson, I. Petkovic, V. Schaller, M. J. W. Rodwell, C. M. Marcus, P. Krogstrup, L. P. Kouwenhoven, E. P. A. M. Bakkers, and C. J. Palmstrom, Phys. Rev. Mater. **3**, 084606 (2019).
[33]Y. Jiang, S. Yang, L. Li, W. Song, W. Miao, B. Tong, Z. Geng, Y. Gao, R. Li, F. Chen, Q. Zhang, F. Meng, L. Gu, K. Zhu, Y. Zang, R. Shang, Z. Cao, X. Feng, Q.-K. Xue, D. E. Liu, H. Zhang, and K. He, Phys. Rev. Mater. **6**, 034205 (2022).
[34]J. Jung, S. G. Schellingerhout, M. F. Ritter, S. C. ten Kate, O. A. H. van der Molen, S. de Loijer, M. A. Verheijen, H. Riel, F. Nichele, and E. P. A. M. Bakkers, Adv. Funct. Mater. **32**, 2208974 (2022).
[35]L. Wen, D. Pan, L. Liu, S. Tong, R. Zhuo, and J. Zhao, J. Phys. Chem. Lett. **13**, 598 (2022).
[36]L. Liu, L. J. Wen, F. Y. He, R. Zhuo, D. Pan, and J. H. Zhao, Nanotechnology **35**, 065705 (2024).
[37]L. Persichetti, M. Fanfoni, M. De Seta, L. Di Gaspare, L. Ottaviano, C. Goletti, and A. Sgarlata, Appl. Surf. Sci. **462**, 86 (2018).
[38]L. Persichetti, A. Sgarlata, S. Mori, M. Notarianni, V. Cherubini, M. Fanfoni, N. Motta, and A. Balzarotti, Nanoscale Res. Lett. **9**, 358 (2014).
[39]Y. Zhang, C. Zhou, Y. Zhu, G. Xia, L. Li, and R.-T. Wen, J. Appl. Phys. **133**, 075703 (2023).
[40]T. M. Diallo, M. R. Aziziyan, R. Arvinte, R. Ares, S. Fafard, and A. Boucherif, Carbon **174**, 214 (2021).
[41]H. Wang, Z. Zhang, L. M. Wong, S. Wang, Z. Wei, G. P. Li, G. Xing, D. Guo, D. Wang, and T. Wu, ACS Nano **4**, 2901 (2010).
[42]D. Rajska, A. Brzozka, M. Marciszko-Wiackowska, M. M. Marzec, D. Chlebda, K. E. Hnida-Gut, and G. D. Sulka, Appl. Surf. Sci. **537**, 147715 (2021).
[43]R. Xu, K. Xu, Y. Sun, Y. Wen, L. Cheng, F.-C. Shen, and Y. Qian, Nanoscale **15**, 18473 (2023).
[44]A. Patra, J. K. Panda, A. Roy, M. Gemmi, J. David, D. Ercolani, and L. Sorba, Appl. Phys. Lett. **107**, 093103 (2015).
[45]G. Faraci, S. Gibilisco, P. Russo, A. R. Pennisi, and S. La Rosa, Phys. Rev. B **73**, 033307 (2006).
[46]G. Gouadec and P. Colomban, Prog. Cryst. Growth Charact. Mater. **53**, 1–56 (2007).
[47]W. Shi, X. Zhang, X.-L. Li, X.-F. Qiao, J.-B. Wu, J. Zhang, and P.-H. Tan, Chin. Phys. Lett. **33**, 057801 (2016).
[48]S. Rohmfeld, M. Hundhausen, and L. Ley, Phys. Rev. B **58**, 9858 (1998).
[49]K. Fujita, Y. Kusumi, and M. Ichikawa, Surf. Sci. **380**, 66 (1997).
[50]Z. Xue, M. Sun, T. Dong, Z. Tang, Y. Zhao, J. Wang, X. Wei, L. Yu, Q. Chen, J. Xu, Y. Shi, K. Chen, and P. Roca i Cabarrocas, Nano Lett. **17**, 7638 (2017).
[51]H. Kim, C. Mattevi, M. R. Calvo, J. C. Oberg, L. Artiglia, S. Agnoli, C. F. Hirjibehedin, M. Chhowalla, and E. Saiz, ACS Nano **6**, 3614 (2012).
[52]A. Lin, J. N. Shapiro, H. Eisele, and D. L. Huffaker, Adv. Funct. Mater. **24**, 4311 (2014).